

Unmanned Aerial Survey for Modelling Glacier Topography in Antarctica: First Results

Dmitrii Bliakharskii^{1,2} and Igor Florinsky²

¹*Institute of Earth Sciences, St. Petersburg University, 199034, St. Petersburg, Russian Federation*

²*Institute of Mathematical Problems of Biology, Keldysh Institute of Applied Mathematics, Russian Academy of Sciences, 142290, Pushchino, Moscow Region, Russian Federation*

Keywords: Unmanned Aerial System, Unmanned Aerial Vehicle, Photogrammetry, Digital Elevation Model, Crevasse.

Abstract: For Antarctic research, one of the most important support tasks is a rapid and safe monitoring of sledge routes, snow / ice airfields, and other visited areas for detection of open crevasses, revealing of hidden, snow-covered ones, as well as studying of their dynamics. We present the first results from a study of applying unmanned aerial systems (UASs) and UAS-derived data to model glacier topography in contexts of detecting crevasses and monitoring changes in glacier surfaces. The study was conducted in East Antarctica in the austral summer 2016/2017. The surveyed areas included an eastern part of the Larsemann Hills, an airfield of the Progress Station, an initial section of a sledge route from the Progress to Vostok Stations, and a north-western portion of the Dâlk Glacier before and after its collapse. The surveying was performed by Geoscan 201, a flying-wing UAS. For the photogrammetric processing of imagery, we applied software Agisoft PhotoScan Professional. High-resolution digital elevation models (DEMs) for surveyed areas were produced. For the Dâlk Glacier, we derived two DEMs related to the pre- and post-collapse glacier surface. A further analysis will be performed by methods of geomorphometry. The focus will be on the revealing of crevasses.

1 INTRODUCTION

Unmanned aerial systems (UASs) are increasingly used in sciences and industry (Aber et al., 2010; Colomina and Molina, 2014; Shahbazi et al., 2014; Pajares, 2015; Toth and Józkw, 2016). In particular, UAS-derived imagery is utilized for producing high-resolution digital elevation models (DEMs), which are then applied, e.g., to study and model dynamics of slope, coastal, and fluvial processes, to reveal fine geological features, etc. (Smith et al., 2009; D'Oleire-Oltmanns et al., 2012; Mancini et al., 2013; Bemis et al., 2014; Johnson et al., 2014; Brunier et al., 2016; Florinsky et al., 2018).

The use of UASs may significantly facilitate the work of researchers in severe conditions of high mountain glaciers and ice sheets (see a review of UAS application in glaciology — Bhardwaj et al., 2016). In Antarctica, UAS-derived data including DEMs are used for geomorphological and vegetation studies and surface evolution analysis (Lucieer et al., 2014; Westoby et al., 2015; Dąbski et al., 2017).

Extreme temperature and meteorological conditions of Antarctica make special demands on the characteristics of UASs, installed equipment, and aerial surveying techniques (Funaki and Hirasawa, 2008; Crocker et al., 2011; Goetzendorf-Grabowski and Rodzewicz, 2017).

The glaciers of Antarctica are in continuous motion. As a particular result, crevasses constantly form on the surface and in the near-surface layer of glaciers (Van der Veen, 1999; Colgan et al., 2016). Crevasses pose a significant danger to polar explorers. Thus, for Antarctic research, one of the most important support tasks is a rapid and safe monitoring of sledge routes, airfields (snow / ice runways and skiways), and other visited areas for detection of open crevasses, revealing of hidden (snow-covered) ones, as well as studying of their dynamics. For real-time detection and revealing of crevasses, ground penetration radars are usually applied, with antennas mounted in front of the moving vehicle (for a detailed review of approaches for crevasse detection, see Colgan et al., 2016, pp. 15–20). Although aerial imagery may be utilized to

monitor crevasses and their dynamics, a rapid aerial survey from manned aircrafts is not always possible due to its high cost as well as weather and lighting conditions. Moreover, aerial photographs of glacier surfaces cannot always be interpreted because of specific conditions for image formation, such as low contrast of scenes, glare from snow and ice surfaces.

UASs introduce a low-cost alternative to manned aerial survey. The processes of crevasse formation and propagation are reflected in the geometry of a glacier surface. So, to reveal crevasses and monitor glacier surfaces, it might be possible to use secondary products of unmanned aerial survey, that is, DEMs derived from stereo images. In this paper, we present the first results from a study of applying unmanned aerial survey and UAS-derived data to model glacier topography in Antarctica in contexts of detecting crevasses and monitoring changes in glacier surfaces under austral summer conditions.

2 STUDY AREAS

The study was conducted in and near the Larsemann Hills, East Antarctica (Figure 1). The Larsemann Hills are ice-free, low rounded hills with an area of about 40 sq km located on the south-eastern coast of the Prydz Bay, Princess Elizabeth Land (Stüwe et al., 1989). This coastal oasis includes Stornes and Broknes peninsulas, four small peninsulas, and about 130 islands. The Larsemann Hills is one of the Antarctic Specially Managed Area (ATCM, 2014). There are three year-round operated polar stations in this area: Progress (Russia), Zhongshan (China), and Bharati (India).

There were four surveyed areas (Figure 1):

- An eastern part of the Larsemann Hills.
- An airfield (skiway) of the Progress Station located on the ice plateau south of the Larsemann Hills.
- An initial section (from 69°27'24" S, 76°19'04" E to 69°40'40" S, 76°32'46" E) of a sledge route from the Progress to Vostok Stations.
- A north-western portion of the Dalk Glacier.

The Dalk Glacier is a 15-km long, polar outlet glacier draining into the south-eastern part of the Prydz Bay east of the Larsemann Hills. On January 30, 2017, a rare natural catastrophic phenomenon occurred: a wide collapsed depression formed in the north-western margin of this glacier, at coordinates 69°23'58" S, 76°24'49" E (Popov et al., 2017).

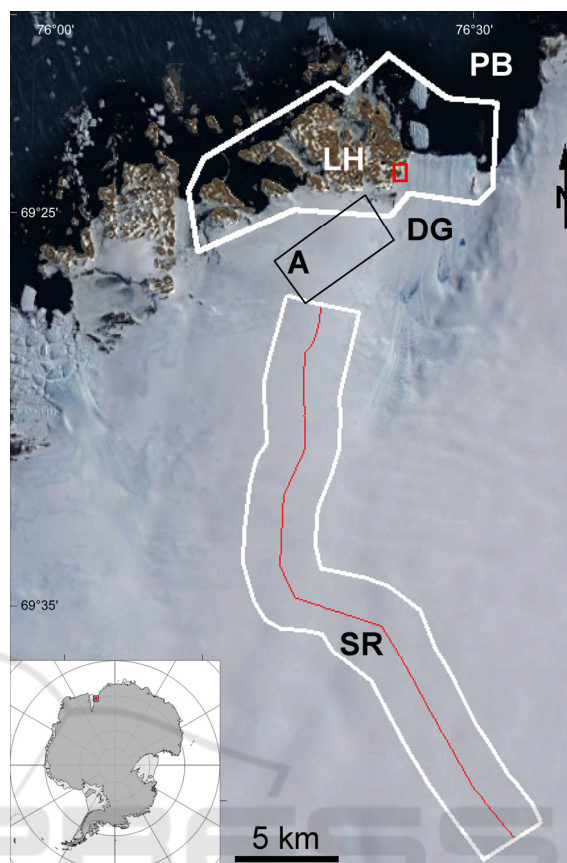


Figure 1: Geographical location of the surveyed areas on the background of the Google Earth image mosaic: the white frame LH — the eastern part of the Larsemann Hills (see Figure 3); the black frame A — the airfield area (see Figure 4); the white frame SR — the area of the initial section of the sledge route (the red line) from the Progress to Vostok Stations (see Figure 5); the red frame marks the area of a collapsed portion of the Dalk Glacier (see Figure 7); DG — Dalk Glacier, PB — Prydz Bay.

3 UAS CHARACTERISTICS

The surveying was performed by Geoscan 201 (Figure 2), a flying-wing UAS, with a wingspan of 2.3 m and a takeoff weight of 8 kg, launching by a catapult and landing with a parachute (Geoscan, 2016). Geoscan 201 has an electric motor; the flight duration is up to 2.5 hrs with a cruising speed of 110 km/h. On board there are:

- A modem for the telemetry communication with a laptop ground control station (GCS).
- A visible-band digital camera Sony DSC-RX1 equipped with a Carl Zeiss Vario Sonnar T lens (central shutter; 35 mm focal length) and



Figure 2: A UAS Geoscan 201 (Geoscan, 2016).

a 35.8×23.9 mm sensor (a matrix of 6000×4000 pixels with pixel sizes of 6×6 μm).

- A GNSS receiver Topcon for high-precision determination of image projection centres.

A ground GNSS base station includes a receiver Topcon HiPer V.

To consider the lens distortion, we previously performed a laboratory photogrammetric calibration of the camera, as well as a field camera calibration. The following camera settings are used during an aerial survey: (1) the lens is locked to focus to infinity; (2) the shutter priority are 1/1000 and 1/800 seconds for sunny and cloudy weather, correspondingly; (3) an aperture and ISO sensitivity values are selected automatically, one time per a flight stripe; (4) images are recorded as JPEG files.

The combination of the mentioned camera and GNSS receiver allows determining image projection centres with the planimetric and vertical accuracies of 2 cm and 3–4 cm, correspondingly.

The Geoscan 201 flight is performed in an automatic mode using an autopilot. One should specify a flight mission in the GCS by selecting a surveyed area and setting flight parameters. The key parameter is an overlap between images. It is recommended to set 70 % forward and 50 % side overlaps. Then, one of the three interrelated parameters should be set: ground sample distance, flight altitude, and strip width. Flights can be conducted either at a constant altitude above ground level (AGL) or a constant altitude above sea level. We used the first option. Finally, a GCS program calculates the flight stripes and coordinates of image capture positions.

Before sending the Geoscan 201 to Antarctica, it was modernized as follows: (1) a filament was built into the camera lens to evaporate the possible condensate when passing through 0°C ; (2) a self-heating function was embedded in the rechargeable batteries; and (3) the rubber catapult was supplemented by a spring.

Table 1: Flight characteristics.

Date	Flight	Flight altitude (m AGL)	Number of flight stripes	Number of images
Larsemann Hills				
14.01	2	370–410	19	1,089
–"–	3	–"–	26	1,230
20.01	14	310–350	20	1,594
–"–	15	–"–	34	1,538
Total			99	5,451
Airfield				
14.01	1	520	16	856
14.02	30	390	17	1,271
Sledge route				
17.01	5	400–430	26	1,280
–"–	6	–"–	32	1,484
–"–	7	300–320	23	1,428
–"–	8	–"–	25	1,260
18.01	9	–"–	16	766
–"–	10	–"–	11	535
–"–	11	–"–	24	1,025
–"–	12	–"–	17	800
–"–	13	400–430	21	803
Total			195	9,381
03.02	20	400–430	21	813
–"–	21	–"–	21	1,053
04.02	23	300–320	29	1,400
–"–	24	–"–	26	1,614
–"–	25	–"–	29	1,316
Total			126	6,196
Dålk Glacier, collapsed area				
20.01	14	310–350	20	1,594
09.02	29	320–330	30	1,011

4 AERIAL SURVEYING

The aerial survey was conducted in January and February 2017 under various meteorological conditions including clear sunny weather, variable cloudiness, and overcast. The air temperature ranged from -1°C to -12°C . The wind speed varied from 0 m/s to 28 m/s at the flight altitude. On and near the coast, the wind was northeast. On the ice sheet, the wind was south katabatic in morning and north afternoon. General flight characteristics are summarized in Table 1.

The eastern part of the Larsemann Hills with an area of about 67 sq km (Figure 3a) was surveyed in four flights (Table 1). The weather was sunny; the air temperature ranged from -1°C to -5°C ; the wind speed was up to 5 m/s at the flight altitude. Totally, the aerial survey consisted of 99 flight stripes including 5,451 images.

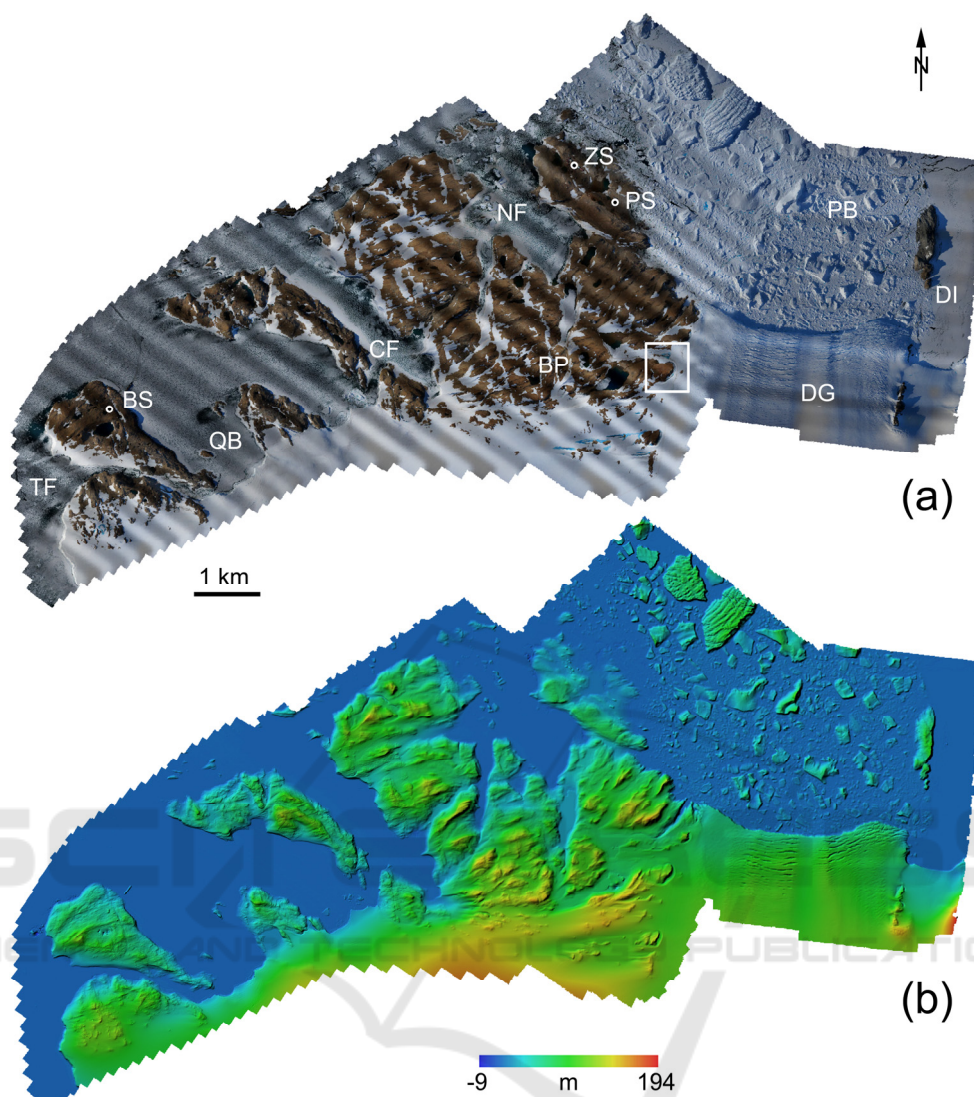


Figure 3: The eastern part of the Larsemann Hills: (a) orthomosaic; (b) elevations. BP — Broknæs Peninsula, PS — Progress Station, ZS — Zhongshan Station, BS — Bharati Station, DG — Dalk Glacier, PB — Prydz Bay, QB — Quilty Bay, TF — Thala Fjord, CF — Clemence Fjord, NF — Nella Fjord, DI — Dalkøya Island; the white frame marks the area of a collapsed portion of the Dalk Glacier (see Figure 7).

The airfield area of about 10 sq km (Figure 4a) was surveyed twice — in mid-January and mid-February — to estimate the snow melting (Table 1). During the first flight, the weather was sunny; the air temperature ranged from $-3\text{ }^{\circ}\text{C}$ to $-5\text{ }^{\circ}\text{C}$; the wind speed was 3–5 m/s at the flight altitude. The first survey consisted of 16 flight stripes including 856 images. During the second flight, it was variable, mid-level cloudiness; the air temperature was $-8\text{ }^{\circ}\text{C}$; the wind speed was about 10 m/s at the flight altitude. The second survey consisted of 17 flight stripes including 1,271 images.

The area of the initial section of the sledge route

from the Progress to Vostok Stations with a length of about 30 km and a width of around 3 km (Figure 5a) was surveyed twice — in mid-January and early February — to estimate the ice movement. As ground control points, we used 17 plastic stakes and 10 barrels. During the first and second surveys, we performed nine and five flights, correspondingly (Table 1). During the first survey, the weather was sunny; the air temperature ranged m/s gusting up to 18–20 m/s at the flight altitude. The surveyed area was about 102 sq km. The first survey consisted of 195 flight stripes including 9,381 images. During the second survey, weather conditions deteriorated: it

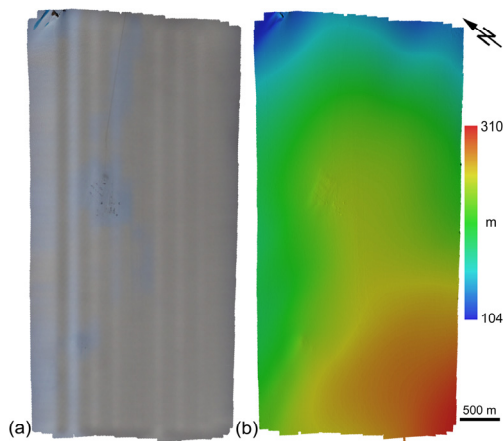


Figure 4: The airfield area (mid-January): (a) orthomosaic; (b) elevations.

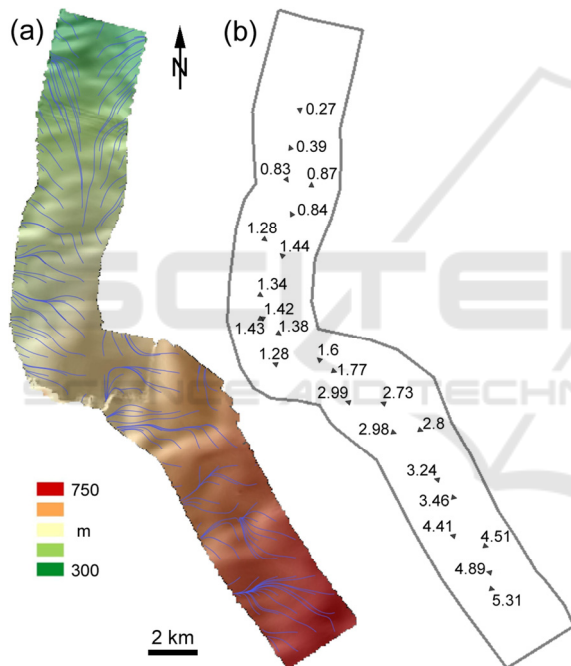


Figure 5: The area of the initial section of the sledge route from the Progress to Vostok Stations (mid-January): (a) elevations and thalweg lines; (b) ice movement (meters). Arrows show the direction of movement.

was overcast with a cloud base of about 1000 m; the air temperature ranged from $-7\text{ }^{\circ}\text{C}$ to $-12\text{ }^{\circ}\text{C}$; the wind speed was 15–20 m/s gusting up to 25–28 m/s at the flight altitude. In this connection, it was impossible to perform aerial surveying of the entire study area (the surveyed area was about 73 sq km). The second survey consisted of 126 flight stripes with 6,196 images (Figure 6).

The collapsed portion of the Dâlk Glacier and an

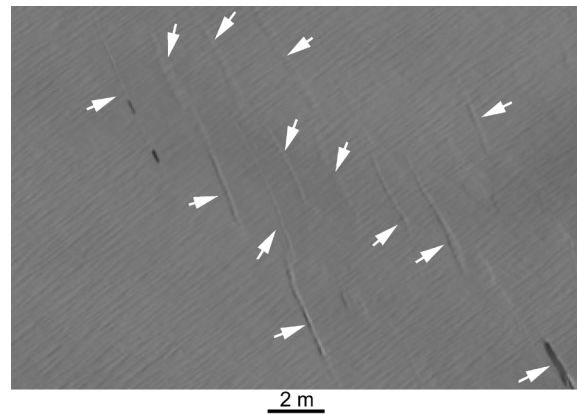


Figure 6: An example of aerial photographs of the sledge route area. Arrows mark crevasses.

adjacent territory with an area of about 7.5 sq km (Figure 7a) was surveyed in two flights, before and after the glacier's collapse (Table 1). The weather was sunny; the air temperature ranged from $-1\text{ }^{\circ}\text{C}$ to $-5\text{ }^{\circ}\text{C}$; the wind speed was 0–5 m/s at the flight altitude. The aerial surveying consisted of 20 and 30 flight stripes including 1,594 and 1,011 images for the first and second flights, correspondingly.

Each flight took about 2 hrs. For all flights, forward and side overlaps were about 70 % and 50 %, correspondingly. Aerial images have the average resolution of 6 cm.

We described only those aerial surveys, which images were then successfully processed (Section 5). Testing flights were also conducted. It has been empirically found that in Antarctica, it is advisable to perform unmanned aerial survey in sunny weather, at variable and high cloudiness (5–6 km AGL). On contrast images captured in such a good lighting conditions, microtopographic ice features created by the wind are clearly visible on the ice surface. A correlation algorithm uses these ice microfeatures for searching conjugate points in the photogrammetric processing of images (Section 5). Under low cloudiness and hence diffuse lighting, one obtains low-contrast, almost white aerial photographs, which are difficult or impossible to process because ice microfeatures are not visible.

It is absolutely impossible to perform unmanned aerial survey under low clouds (100–200 m AGL). In this case, whiteout occurs when there is no contrast between ice- and snow-covered terrain and sky, that is, ice, sky, and horizon are indistinguishable.

Sometimes, it was difficult to determine the cloud height. As a result, the UAS went into the clouds. In these cases, the UAS had ice build-up on the leading edge of wing, Pitot tube, and screw

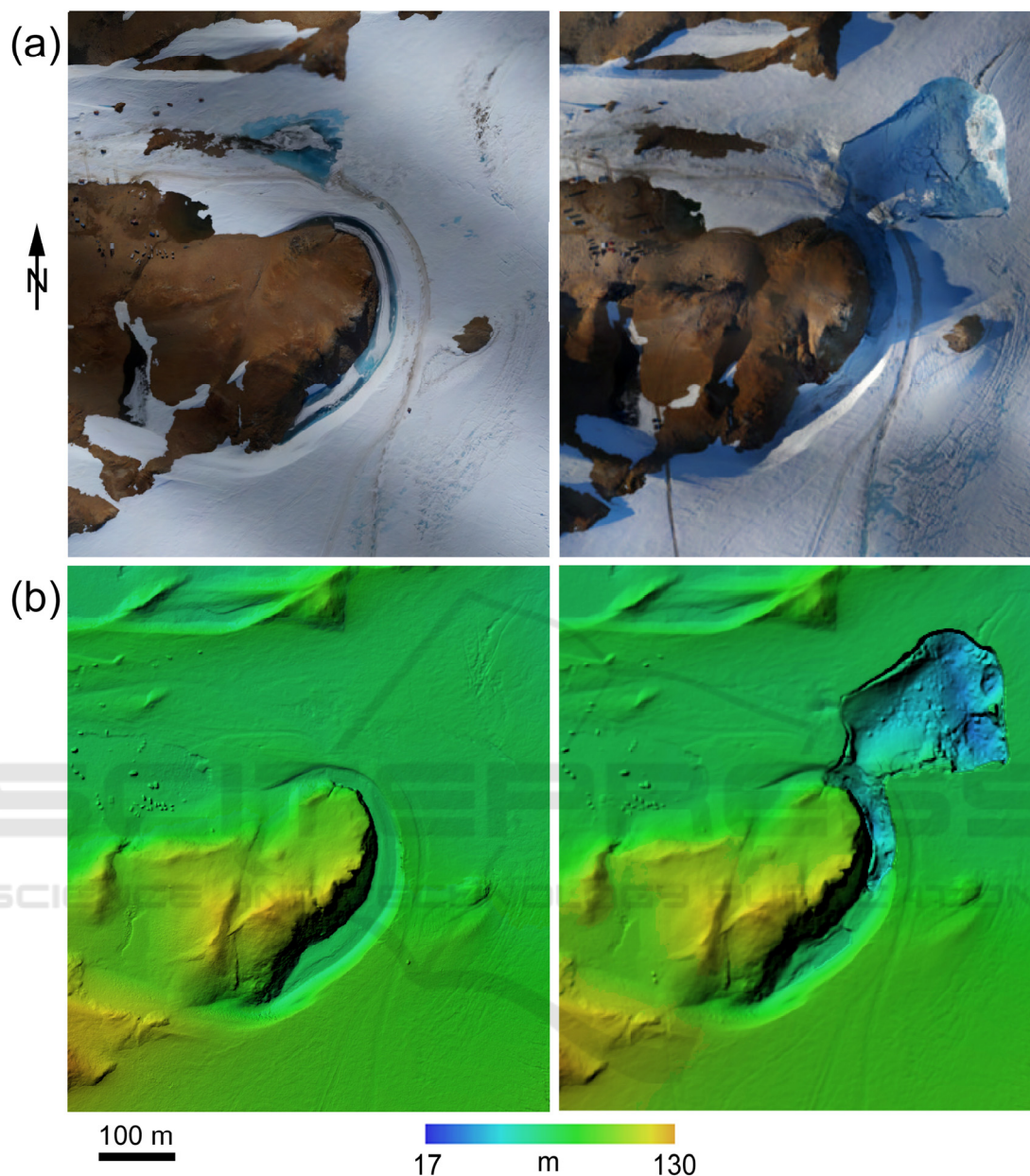


Figure 7: The north-western margin of the Dâlk Glacier before (left) and after (right) the surface collapse (for the location of this area, see Figures 1 and 3): (a) orthomosaics; (b) elevations.

blades that led to an increase in UAS’s weight and its emergency landing.

5 IMAGE PROCESSING

The image processing consisted of two stages: (1) a post-processing of the on-board GNSS receiver measurements relative to the base station; and (2) a photogrammetric processing of the aerial images.

For the first stage, we used Pinnacle software (Topcon Positioning Systems, Inc.). We positioned images with corresponding coordinates of image projection centres. The coordinates were utilized in the next stage as reference data.

For the second stage, we used Agisoft PhotoScan Professional 1.3.2 software (Agisoft, 2017). This choice is determined by the fact that Geoscan 201 and Agisoft PhotoScan represent a unified software–hardware system (Inozemtsev, 2014). This software implements a set of traditional photogrammetric

Table 2: Accuracy of the aerial triangulation in terms of standard deviation.

Area	Planimetric (m)		Vertical (m)
	X	Y	
Larsemann Hills	0.09	0.12	0.08
Airfield	0.05	0.04	0.03
Sledge route	1.9	0.5	0.8
Dålk Glacier, collapsed zone	0.05	0.05	0.06

Table 3: DEM characteristics.

Area	Matrix size	Resolution (m)
Larsemann Hills	68,913 × 41,879	0.28
Airfield	30,991 × 26,771	0.27
Sledge route	12,817 × 19,082	1.9
Dålk Glacier, collapsed zone	8,400 × 7,655	0.22

methods (Kraus, 2007; Mikhailov and Chibunichev, 2016) and structure-from-motion approaches (Hirschmüller, 2008; Smith et al., 2016).

The image processing is based on an algorithm developed in Agisoft (2017). The brightness of images is analysed, so that a large number of conjugate points are defined on overlapping images. Using conjugate points, the parameters of image orientation and lens distortion are determined. Using reference points, a photogrammetric model, derived from all images of the block, becomes a metric one. Thus, the block aerial triangulation is performed. For accuracy of the aerial triangulation, see Table 2.

Densifying a cloud of conjugate points to a dense point cloud using all obtained elements, one can obtain an irregular digital surface model (DSM). Then, one can derive a regular DSM from the irregular one by linear interpolation. In a general case, when the dense point cloud is obtained, one can produce a DEM by applying a classification algorithm developed by Agisoft (2017). Recall that a DEM describes the topographic surface while a DSM represents a surface enveloping or consisting of portions of the topographic surface, vegetation canopy, top of buildings, and other objects located on the topographic surface. However, in this study, a DSM can be considered a DEM for almost all areas (except for very small zones including polar station's buildings).

Using obtained aerial imagery, we generated high-resolution DEMs (Figures 3b, 4b, 5a, and 7b). For the airfield area, we derived two DEMs related to mid-January and mid-February dates of survey. For the initial section of the sledge route, two DEMs related to mid-January and early February dates of

survey were also produced. For the north-western margin of the Dålk Glacier, we derived two DEMs related to the pre- and post-collapsed glacier surface (Figure 7b). General characteristics of the DEMs can be found in Table 3. Notice that the DEMs of the Larsemann Hills (Figure 3b) and the Dålk Glacier (Figure 7b) describe mixed surfaces of the bedrock and ice. The DEMs of the airfield area and the sledge route describe the ice surface only.

Accuracy estimation of the obtained DEMs is a non-trivial task. Usually, it can be solved using GCPs with known planimetric coordinates and elevation values. However, in this study it was impossible to set up GCPs at all glacier areas due to safety issues. At the sledge route, we set up 27 GCPs, but these cannot be used for the DEM accuracy estimation because of a high speed of the ice movement and a time gap between geodetic and aerial works (GCPs moved together with the ice). On the initial section of the sledge route, the ice movement ranged from 0.28 m to 5.31 m in 21 days between the first and second surveys (Figure 5b), that is, up to 0.25 m per day. For a rough estimation of the DEM accuracy, one may use data for the accuracy of the aerial triangulation (Table 2).

6 CONCLUSIONS

We studied possibilities of applying a small UAS and UAS-derived images to model glacier topography in Antarctica. Optimal meteorological conditions were empirically determined for conducting unmanned aerial survey to obtain images suitable for subsequent photogrammetric processing and DEM generation. For four areas, high-resolution DEMs of bedrock/glacier and glacier surfaces were produced. Further analysis of the DEMs will be performed by methods of geomorphometry (Florinsky, 2016). The focus will be on a detailed modelling of the collapsed area of the Dålk Glacier, as well as the revealing of glacier crevasses.

ACKNOWLEDGEMENTS

The aerial surveying was conducted during the 62nd Russian Antarctic Expedition in cooperation with Geoscan Ltd. Data processing is supported by the Russian Foundation for Basic Research, grant 17-37-50011.

REFERENCES

- Aber, J.S., Marzloff, I., Ries, J., 2010. *Small-format aerial photography: Principles, techniques and geoscience applications*. Elsevier, Amsterdam.
- Agisoft, 2017. *Agisoft PhotoScan user manual: Professional edition, version 1.3*. St. Petersburg.
- ATCM, 2014. Larsemann Hills, East Antarctica: Antarctic Specially Managed Area Management Plan. Measure 15. In: *Antarctic Treaty Consultative Meeting (ATCM) XXXVII Final Report*. ATCM.
- Bemis, S.P., Micklethwaite, S., Turner, D., James, M.R., Akciz, S., Thiele, S.T., Bangash, H.A., 2014. Ground-based and UAV-based photogrammetry: A multi-scale, high-resolution mapping tool for structural geology and paleoseismology. *J. Struct. Geol.*, 69: 163-178.
- Bhardwaj, A., Sam, L., Akanksha, Martín-Torres, F.J., Kumar, R., 2016. UAVs as remote sensing platform in glaciology: Present applications and future prospects. *Remote Sens. Environ.*, 175: 196-204.
- Brunier, G., Fleury, J., Anthony, E.J., Gardel, A., Dussouillez, P., 2016. Close-range airborne Structure-from-Motion Photogrammetry for high-resolution beach morphometric surveys: Examples from an embayed rotating beach. *Geomorph.*, 261: 76-88.
- Colgan, W., Rajaram, H., Abdalati, W., McCutchan, C., Mottram, R., Moussavi, M.S., Grigsby, S., 2016. Glacier crevasses: Observations, models, and mass balance implications. *Rev. Geophys.*, 54: 119-161.
- Colomina, I., Molina, P., 2014. Unmanned aerial systems for photogrammetry and remote sensing: A review. *ISPRS J. Photogramm. Remote Sens.*, 92: 79-97.
- Crocker, R.I., Maslanik, J.A., Adler, J.J., Palo, S.E., Herzfeld, U.C., Emery, W.J., 2011. A sensor package for ice surface observations using small unmanned aircraft systems. *IEEE Trans. Geosci. Remote Sens.*, 50: 1033-1047.
- Dąbski, M., Zmarz, A., Pabjanek, P., Korczak-Abshire, M., Karsznia, I., Chwedorzewska, K.J., 2017. UAV-based detection and spatial analyses of periglacial landforms on Demay Point (King George Island, South Shetland Islands, Antarctica). *Geomorph.*, 290: 29-38.
- D'Oleire-Oltmanns, S., Marzloff, I., Peter, K.D., Ries, J.B., 2012. Unmanned aerial vehicle (UAV) for monitoring soil erosion in Morocco. *Remote Sens.*, 4: 3390-3416.
- Florinsky, I.V., 2016. *Digital terrain analysis in soil science and geology*. 2nd ed. Academic Press, Amsterdam.
- Florinsky, I.V., Kurkov, V.M., Bliakharskii, D.P., 2018. Geomorphometry from unmanned aerial surveys. *Trans. GIS*, 22, doi:10.1111/tgis.12296.
- Funaki, M., Hirasawa, N., 2008. Outline of a small unmanned aerial vehicle (Ant-Plane) designed for Antarctic research. *Polar Sci.*, 2: 129-142.
- Geoscan, 2016. *Geoscan 201*. Geoscan Ltd, St.Petersburg, <https://www.geoscan.aero/en/products/geoscan201/bas>
- Goetzendorf-Grabowski, T., Rodzewicz, M., 2017. Design of UAV for photogrammetric mission in Antarctic area. *J. Aerospace Eng.*, 231: 1660-1675.
- Hirschmüller, H., 2008. Stereo processing by semiglobal matching and mutual information. *IEEE Trans. Patt. Anal. Mach. Intell.*, 30: 328-341.
- Inozemtsev, D.P., 2014. Automated aerial survey using a software–hardware system ‘Geoscan–Photoscan’. *CAD & GIS for Roads*, 1(2), 46-51 (in Russian).
- Johnson, K., Nissen, E., Saripalli, S., Arrowsmith, J.R., McGarey, P., Scharer, K., Williams, P., Blisniuk, K., 2014. Rapid mapping of ultrafine fault zone topography with structure from motion. *Geosphere*, 10: 969-986.
- Kraus, K., 2007. *Photogrammetry: Geometry from images and laser scans*, 2nd ed. de Gruyter, Berlin.
- Lucieer, A., Turner, D., King, D.H., Robinson, S.A., 2014. Using an Unmanned Aerial Vehicle (UAV) to capture micro-topography of Antarctic moss beds. *Int. J. Appl. Earth Observ. Geoinf.*, 27: 53-62.
- Mancini, F., Dubbini, M., Gattelli, M., Stecchi, F., Fabbri, S., Gabbianelli, G., 2013. Using unmanned aerial vehicles (UAV) for high-resolution reconstruction of topography: The structure from motion approach on coastal environments. *Remote Sens.*, 5: 6880-6898.
- Mikhailov, A.P., Chibunichev, A.G. (2016). *Photogrammetry*. MIIGAiK, Moscow (in Russian).
- Pajares, G., 2015. Overview and current status of remote sensing applications based on unmanned aerial vehicles (UAVs). *Photogramm. Eng. Remote Sens.*, 81: 281-329.
- Popov, S.V., Pryakhin, S.S., Bliakharskii, D.P., Pryakhina, G.V., Tyurin, S.V., 2017. Vast ice depression in Dalk Glacier, East Antarctica. *Ice Snow*, 57: 427-432.
- Shahbazi, M., Théau, J., Ménard, P., 2014. Recent applications of unmanned aerial imagery in natural resource management. *GISci. Remote Sens.*, 51: 339-365.
- Smith, M.J., Chandler, J., Rose, J., 2009. High spatial resolution data acquisition for the geosciences: Kite aerial photography. *Earth Surf. Process. Landforms*, 34: 155-161.
- Smith, M.W., Carrivick, J.L., Quincey, D.J., 2016. Structure from motion photogrammetry in physical geography. *Progr. Phys. Geogr.*, 40: 247-275.
- Stüwe, K., Braun, H.-M., Peer, H., 1989. Geology and structure of the Larsemann Hills area, Prydz Bay, East Antarctica. *Austral. J. Earth Sci.*, 36: 219-241.
- Toth, C., Józków, G., 2016. Remote sensing platforms and sensors: A survey. *ISPRS J. Photogramm. Remote Sens.*, 115: 22-36.
- Van der Veen, C.J., 1999. Crevasses on glaciers. *Polar Geogr.*, 23: 213-245.
- Westoby, M.J., Dunning, S.A., Woodward, J., Hein, A.S., Marrero, S.M., Winter, K., Sugden, D.E., 2015. Sedimentological characterization of Antarctic moraines using UAVs and Structure-from-Motion photogrammetry. *J. Glaciol.*, 61: 1088-1102.